JOURNAL OF CATALYSIS 127, 227–250 (1991)

Kinetics of the Ammonia Synthesis over Fe/TiO_2, Hydrazine-Pretreated Fe/TiO_2, and Hydrazine-Pretreated Alkali-Promoted Fe/TiO_2 Catalysts

A. NOBILE, JR.,[1] V. VAN BRUNT, AND M. W. DAVIS, JR.

Department of Chemical Engineering, University of South Carolina, Columbia, South Carolina 29225

Received March 27, 1990; revised July 13, 1990

The kinetics of the synthesis of ammonia from its elements over Fe/TiO_2, an hydrazine-pretreated Fe/TiO_2, and hydrazine-pretreated alkali-promoted Fe/TiO_2 catalysts was studied in a flow microreactor at 101 kPa pressure. A significant improvement in the accuracy and precision of kinetic parameters extracted from the data was achieved by modifying the kinetic model to account for deactivation of supported catalyst particles by Ostwald ripening. The modified form of the kinetic model also yielded information about the particle ripening kinetics. Pretreatment of Fe/TiO_2 with hydrazine increased the ammonia synthesis turnover frequency by more than an order of magnitude over unpretreated Fe/TiO_2. The ammonia partial pressure dependence and apparent activation energy over hydrazine-pretreated Fe/TiO_2 were more representative of iron uninfluenced by the strong metal-support interaction (SMSI) which occurs in metal–titania systems. *In situ* CO chemisorption measurements following the ammonia synthesis kinetics measurements showed higher CO uptake with hydrazine-pretreated Fe/TiO_2 than with unpretreated Fe/TiO_2. The increased turnover frequency, altered kinetic parameters, and higher CO uptake suggest that hydrazine pretreatment inhibited the onset of SMSI, which is attributed to titanium nitride formation on the support surface. Addition of the alkali promoters K and Cs to the catalysts not only increased the turnover frequency and decreased the apparent activation energy and ammonia partial pressure dependence, but acted to stabilize supported iron particles against growth by Ostwald ripening. The data suggest that physical covering of the surface by alkali inhibits Ostwald ripening of iron particles by blocking dissociation of iron atoms from supported particles thus suppressing their migration over the support surface to form larger particles.

INTRODUCTION

Previous investigations of the kinetics of ammonia synthesis over supported catalysts has provided much information about the catalytically active phase and the influence of the support on the catalytic properties of the active phase. An important contribution to this area was the discovery by the Stanford group that the ammonia synthesis turnover frequency depends strongly on the size and pretreatment of iron particles supported on magnesia (*1–4*). This, along with other evidence, led to the conclusion that the ammonia synthesis is a structure-sensitive reaction, and that so-called C_7 sites, or surface atoms with sevenfold coordination are the most active for ammonia synthesis. The higher activity of C_7 sites has since been confirmed by studies of the ammonia synthesis over single crystal transition metals (*5–7*). Generally, these studies find that surfaces with more open and rough structures are more active for ammonia synthesis.

The catalytic properties of supported metals are often influenced by interaction with the support. For example, Aika *et al.* (*8*) who studied the ammonia synthesis over ruthenium supported on several supports found the activity to depend strongly on the type of support used. These authors attributed this to variations in the electronic interaction of the metal with the support. Different ammonia synthesis activities and other

[1] Present address: Westinghouse Savannah River Company, Savannah River Laboratory, Bldg. 232-H, Aiken, SC 29808.

0021-9517/91 $3.00

properties were observed by Sueiras *et al.* (*9*) when the degree of alumina protonation of alumina-supported iron catalysts was varied. These studies indicate that the support plays an essential role in the catalytic activity for ammonia synthesis.

Aside from electronic interaction of supported particles with the support, physical phenomena induced by the support may also play a role in the catalytic properties of the supported metal. For example, in the Fe/MgO catalysts investigated by the Stanford group (*1*), interaction of iron particles with the magnesia support was responsible for stabilizing iron particles against high-temperature sintering. In fact, this made possible the investigation of the catalytic properties of small iron particles. Santos *et al.* (*10*) and Santos and Dumesic (*11*), who studied the ammonia synthesis over Fe/TiO_2 catalysts, determined that a small degree of surface poisoning by titania adspecies caused a drastic reduction of ammonia synthesis activity. Apparently, since sites for ammonia synthesis are comprised of a large ensemble of surface atoms, a small degree of surface poisoning has a large effect on the catalytic activity. These same workers also showed that the catalytic properties of the supported iron particles were altered by electronic modification from titania adspecies on the particle surfaces.

For many years, it has been known that alkali metals provide a promoter effect on the ammonia synthesis reaction on iron catalysts (*12*). Investigations of alkali promoters over single crystal transition metals have provided detailed information about the mechanism by which alkali promoters increase ammonia synthesis rates (*13–16*). Apparently, electrons transferred from adsorbed alkali to the transition metal surface increase electron donation from the metal to adsorbed nitrogen antibonding orbitals, facilitating cleavage of the dinitrogen bond. Reduction of the work function of the transition metal after promotion with alkali (*13–15*), increased adsorption energy of molecular nitrogen, and decreased activation energy for N_2 dissociation (*16*) support this picture.

While the behavior of such model systems is fairly well understood, the effects of alkali promoters in supported catalysts, which are of potential industrial interest, are less well understood. Here, the phenomena are more complex since the catalytic properties of the active phase are influenced not only by the promoter, but also by the support. Aika *et al.* (*8, 17*) observed large increases in ammonia synthesis activity when alkali metals were added to transition metals on several supports. An interesting finding of the work of Aika *et al.* (*8*) was that while activated carbon-supported ruthenium exhibited the lowest activity of the unpromoted catalysts, when promoted, activated carbon-supported ruthenium had the highest activity. This indicates that aside from influencing the properties of the supported particles, the support may influence the manner by which alkali promotes the supported particles. This is quite interesting, and it suggests that an optimum combination of support type and promoter could produce a very active catalyst for ammonia synthesis. Thus, the alkali promoter effect on the ammonia synthesis reaction in supported catalysts deserves further study.

Previous investigations of the ammonia synthesis over alkali-promoted supported catalysts have demonstrated the promoter effect on the reaction, but have not determined kinetic parameters which could yield fundamental information about the promoter effect. The aim of this study was to investigate the ammonia synthesis kinetics over Fe/TiO_2, hydrazine-pretreated Fe/TiO_2, and hydrazine-pretreated alkali-promoted Fe/TiO_2 catalysts. Kinetic parameters in the Temkin–Pyzhev model and turnover frequencies were determined for each catalyst. The kinetic model used to analyze the data was modified to account for deactivation of the catalysts by Ostwald ripening of supported particles. This improved the accuracy and precision of the kinetic parameters extracted from the data, and yielded

information about the kinetics of particle growth. X-ray diffraction and *in situ* CO chemisorption were used to further characterize the catalysts.

METHODS

Catalyst preparation. All catalysts were prepared using Degussa P-25 TiO_2. X-ray diffraction analysis of the pure material indicated that it was about 15% rutile, 85% anatase. Catalyst samples were prepared by incipient wetness impregnation with saturated solutions of $Fe(NO_3)_3 \cdot 9H_2O$ (99.997%, Aldrich) in dimethyl formamide (DMF). DMF was chosen over aqueous acid as an impregnating solvent, since we have previously shown that higher iron dispersion results with DMF solutions (*18*). The DMF used was reagent grade, and was obtained from J. T. Baker, Inc. Information obtained from the suppliers on impurities in the reagents indicates that the concentrations of potential poisons (S and P) were low enough to be of no concern. Impregnation was accomplished by dropwise addition of 0.25 ml of solution per gram of titania powder, after which samples were air-dried at 393 K for 24 h. Two successive impregnations in this manner yielded catalysts with composition near 7 wt% iron. Catalysts promoted with potassium and cesium were prepared by subsequently adding 0.3 ml per gram of powder of a solution of the desired alkali nitrate salt (reagent grade, J. T. Baker, Inc.) in doubly distilled water, followed by air drying of the impregnates at 393 K for 24 h. The alkali concentration in the solution was adjusted to yield 1 promoter atom to 10 iron atoms in the catalyst.

Catalysts pretreated with hydrazine (Olin) were pretreated under inert nitrogen atmosphere. Accordingly, impregnated samples (ca. 5 g) were placed in an evacuable glass cell which could be continuously purged with nitrogen during hydrazine pretreatment. The cell was equipped with a rubber septum through which hydrazine was added with a syringe. Enough hydrazine (ca. 6 ml) was added to completely wet the catalyst. This was allowed to stand for 12 h under slow nitrogen purge. The pretreated catalyst was then dried by evacuating for 8 h to a pressure of 10^{-2} Pa. It was then removed from the cell, sieved to the desired particle size, and transferred to the reactor.

The iron composition in the catalysts was determined by inductively coupled plasma (ICP) spectroscopic analysis of solutions obtained by dissolution of catalyst samples in an HF/H_2SO_4 mixture. The alkali content was measured by flame atomic emission spectrometry.

Ammonia synthesis kinetics measurements. Ammonia synthesis kinetics measurements were conducted at 101 kPa pressure in a greaseless glass high-vacuum flow microreactor apparatus which was capable of measuring the number of surface iron atoms in the catalyst by *in situ* CO chemisorption. A chemisorption measurement which immediately followed each ammonia synthesis kinetics measurement determined the number of active catalyst sites in the reactor, allowing rates to be expressed as turnover frequency (NH_3 molecules produced $site^{-1}\ s^{-1}$). During ammonia synthesis kinetics measurements, the catalyst (ca. 3.2 g) was contained in the quartz microreactor/chemisorption cell shown in Fig. 1. Catalyst samples which were sieved to yield particles having diameters in the range 250–420 μm were supported in the cell by a quartz frit. The catalyst bed was 12 mm in diameter by 35 mm long. A 3-mm-diameter quartz thermowell containing a 1-mm-diameter thermocouple protruded into the upper part of the bed for measurement and control of the reactor temperature. During heating the cell was placed in a tube furnace where a temperature controller maintained its temperature to within 0.5 K. The long narrow inlet section of the microreactor/chemisorption cell was packed with 590–840 μm quartz granules to reduce free-volume for chemisorption measurements and to provide preheating for incoming gases during ammonia synthesis kinetics measurements. By placement of the thermocouple at differ-

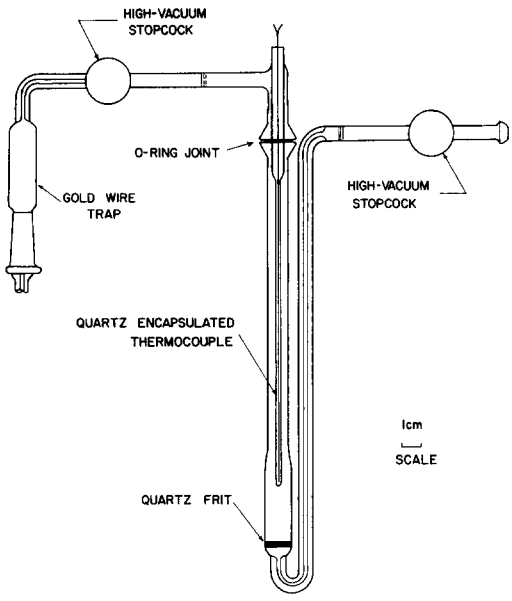

FIG. 1. Quartz microreactor/chemisorption cell.

ent axial positions along the inlet section of the reactor, it was observed that at the highest flow rate used in the ammonia synthesis kinetics measurements (2.8 ml STP s^{-1}), the incoming gas reached the bed temperature before entering the bed.

Reduction of the catalyst before the ammonia synthesis kinetics measurements consisted of 2 h flowing hydrogen (1.7 ml STP s^{-1}) at 393 K, followed by 24 h flowing hydrogen (1.7 ml STP s^{-1}) at 693 K. Other investigators (*10, 19*) have determined that iron supported on titania reaches near full reduction under similar conditions. Hydrogen (99.995%, Airco) was further purified by passage through an Engelhard Deoxo purifier, followed by passage through molecular sieves immersed in liquid nitrogen. After hydrogen reduction a 75% H_2, 25% N_2 stoichiometric feed mixture (99.998%, Airco) was introduced and allowed to flow through the bed (1.7 ml STP s^{-1}) for 16 h at 693 K to establish steady-state ammonia production. This mixture was purified in the same manner as the hydrogen, with the exception that the molecular sieves were immersed in a dry ice–acetone slurry. Flow rate was measured quantitatively with a soap bubble flowmeter located downstream of the reactor. Ammonia concentration in the reactor effluent was measured by passing the stream through a scrubber which contained 25 ml of a 10^{-3} *M* HCl solution and a mixed indicator prepared from methyl red and bromcresol green indicators (*20*). The ammonia concentration was determined by measuring the time required to neutralize the acid solution. Experiments were performed to assure that all ammonia was removed from the gas stream by the scrubber. Varying the flow rate between 1 and 3.2 ml STP s^{-1}, it was determined (using a Matheson certified standard calibration gas) that the ammonia partial pressure remained constant. In addition, the volume of solution in the scrubber was increased from 25 to 50 ml, and the same value for the ammonia partial pressure was obtained. The partial pressures measured with the scrubber differed from the calibration gas analysis by about 3%.

Ammonia synthesis kinetics measurements consisted of setting a temperature in the range 644–693 K, and allowing the establishment of steady state for 8 h while flowing the feed mixture at a rate of 1.7 ml STP s^{-1}. The ammonia concentration in the reactor effluent was then measured at 4–6 randomly chosen flow rates in the range 1.5–2.8 ml STP s^{-1}. The reaction was carried out at four or five temperatures in the above range in a random manner. Application of the criteria established by Mears (*21*) indicated that the kinetic data were uninfluenced by heat and mass transfer effects. The results of this analysis and other details about the apparatus are documented elsewhere (*22*).

Carbon monoxide chemisorption. An *in situ* CO chemisorption measurement was performed immediately following each ammonia synthesis kinetics measurement to determine the number of surface metallic iron atoms in the reactor. The CO chemisorption method was similar to the one developed by Emmett and Brunauer (*23, 24*), and used by others (*1, 10*). At the comple-

tion of each ammonia synthesis kinetics measurement, the sample temperature was set to 673 K and hydrogen (purified as above) was flowed (1.7 ml STP s^{-1}) through the catalyst bed for 1 h to remove nitrogen-containing species from the iron surface. The cell was then evacuated to 10^{-4} Pa for 3 h at 673 K to remove chemisorbed hydrogen. The sample was chilled to 193 K (dry ice–acetone) and the chemisorption measurement was then performed. Accordingly, a CO adsorption isotherm at 193 K was first obtained by dosing small aliquots of CO into the cell and measuring the equilibrium pressure with a Texas Instruments Model 145 precision gage. The sample was then warmed to 273 K and evacuated for 1 h at 10^{-3} Pa to remove physisorbed CO. A second isotherm was then obtained at 193 K. The difference between the two isotherms at 13.33 kPA was assumed to be the amount of chemisorbed CO. By performing the same chemisorption measurement for a blank titania sample reduced at 673 K, it was determined that 0.43 μmoles CO g^{-1} were chemisorbed to the support. Thus, this quantity was subtracted from the CO uptake for each catalyst.

Previous investigators have kept the sample temperature at 193 K during the evacuation step to remove physisorbed CO. However, elsewhere (*22*) we have shown that evacuation of physisorbed CO at 193 K is quite slow. Long evacuation periods (>10 h) are required so that CO uptake is not over-predicted. Evacuation at 273 K yields particle sizes calculated from CO chemisorption uptake which are more consistent with those determined by X-ray diffraction line-broadening and transmission electron microscopy (*18*). Cameron and Dwyer (*25*) studied the chemisorption of CO on Fe (100) using X-ray and ultraviolet photoelectron spectroscopies, low-energy electron diffraction, and temperature-programmed desorption. This study indicated that CO is fully associated at temperatures below 300 K and the surface stoichiometry is 2 : 1 Fe : CO. Thus, we were not concerned about CO dissociation at 273 K. The number of surface iron atoms was determined from the chemisorbed CO uptake by assuming a 2 : 1 Fe : CO surface stoichiometry. There is some variation in the surface stoichiometry for different surface crystallographic orientation; however, the available literature data suggests that the 2 : 1 Fe : CO surface stoichiometry is appropriate for supported iron catalysts (*1, 10, 19, 22*). The number of surface iron atoms was used to calculate the turnover frequency and was also used to calculate the surface-average crystallite size, $\langle d_s \rangle$, from the dispersion, D, using the expression $\langle d_s \rangle = 0.9D^{-1}$ (*4*), where $\langle d_s \rangle$ has units of nanometers.

High vacuum for the chemisorption measurements was provided by a mercury diffusion pump backed by a rotary oil pump. Pressures in the vacuum manifold were typically about 10^{-5} Pa. Mercury contamination was prevented by a liquid nitrogen trap between the pump and the vacuum manifold, and an in-line gold wire trap before the sample cell. ICP analysis of several dissolved catalyst samples never detected mercury. Carbon monoxide (99.97%, Linde) was purified by passage through copper turnings held at 473 K followed by passage through molecular sieves immersed in a dry ice–acetone slurry. Helium used for free-volume measurements (99.995%, Airco) was purified in the same manner, with the molecular sieves immersed in liquid nitrogen. These gases were purified before each ammonia synthesis kinetics measurement and were stored in 1-liter glass bulbs so they were readily available.

X-ray diffraction crystallite size. The volume-average size of iron crystallites in the catalysts was determined by X-ray diffraction line-broadening analysis using the Scherrer Equation (*26*). A value of 0.89 was used for the Scherrer constant. The half-height width of the pure diffraction profile was obtained from the half-height width of the measured profile using Warren's correction (*27*). Instrumental broadening needed for Warrens correction was determined by

scanning iron filings which were annealed at 973 K for 48 h. This treatment assured large strain-free iron crystals. The diffractometer was a Philips Model 12215, which utilized Cu $K\alpha$ radiation. Broadening was measured on the (110) α-iron line at $2\theta = 44.71°$. The peak was scanned at a rate of 0.25° min^{-1}.

BET surface area measurement. Total surface areas of catalysts were measured using the BET method with nitrogen as the adsorbate at liquid nitrogen temperature. Immediately following the CO chemisorption measurement the sample was warmed to room temperature and evacuated (ca. 10^{-4} Pa) for 8 h. After the sample was chilled to 77 K, about 15 points on the adsorption isotherm were collected in the P/P_0 range 0.05–0.30. Nitrogen (Linde, 99.998%) was used with no further purification. The surface area was calculated from the monolayer uptake using the value of 0.162 nm^2 $molecule^{-1}$ for the cross-sectional area of a nitrogen molecule (*28*).

RESULTS

Kinetic Model

Data obtained from the ammonia synthesis kinetics measurements were correlated using the Temkin–Pyzhev model (*29*) expressed in terms of partial pressures of reactants and products,

$$r_{NH_3} = k_f P_{N_2} \left(\frac{P_{H_2}^3}{P_{NH_3}^2}\right)^m - k_r \left(\frac{P_{NH_3}^2}{P_{H_2}^3}\right)^{1-m}, \quad (1)$$

where k_f and k_r are forward and reverse rate constants. The value of m is dependent on the nature of the catalyst surface, but is typically in the range 0.5–0.7 for iron catalysts (*29–32*). It has previously been established (*2, 33, 34*) that the rate of the reverse reaction (ammonia decomposition) is negligible when the conversion is less than 10%. In this investigation the conversion never exceeded 4.7%, thus it was justified to neglect the reverse reaction term of Eq. (1). Since the feed mixture composition was constant for all runs, the term $P_{N_2} P_{H_2}^{3m}$ can be absorbed into a pseudo-rate constant, k_f', simplifying the model to

$$r_{NH_3} = k_f' (P_{NH_3})^{-2m}, \quad (2)$$

where $k_f' = k_f P_{N_2} P_{H_2}^{3m}$. Since the ammonia synthesis rate was not constant along the catalyst bed length, analysis of the data required integration of the continuity equation along the catalyst bed length. Since it was desired to obtain rates expressed as turnover frequency, the form of the continuity equation used was

$$-\frac{dN_s}{F_0} = \frac{df_c}{r_{N_2+H_2}}, \quad (3)$$

where N_s is the number of moles of active catalyst sites in the reactor, F_0 is the molar flow rate through the reactor, f_c is the fraction conversion, and $r_{N_2+H_2}$ is the disappearance rate of hydrogen and nitrogen expressed as nitrogen plus hydrogen molecules per second per catalyst site. For small fraction conversions, the ammonia mole fraction, x_{NH_3}, is approximately one-half the fraction conversion. The molecular ammonia formation rate, r_{NH_3}, is minus one-half the molecular disappearance rate of nitrogen and hydrogen. Incorporating these into Eq. (3), the continuity equation takes the form

$$\frac{dN_s}{F_0} = \frac{dx_{NH_3}}{r_{NH_3}} = \frac{1}{P_t}\frac{dP_{NH_3}}{r_{NH_3}}, \quad (4)$$

where P_t is the total pressure. The assumption of the mole fraction being one-half the fraction conversion introduces an error of about 2% at the largest fraction conversion observed in this study and was thus neglected. Inserting Eq. (2) into Eq. (4) and integrating, the following is obtained:

$$\frac{N_s}{F_0} = \frac{1}{k_f' P_t}\left[\frac{(P_{NH_3})^{2m+1}}{2m+1}\right]. \quad (5)$$

This expression provided the basis for correlating data obtained from the ammonia synthesis kinetics measurements. The SAS

NLIN nonlinear regression statistical procedure (*35*) was used to extract the kinetic parameters in the model from the data. Proper use of this statistical procedure required that the dominant experimental error of the measured variables be associated with the dependent variable. Since the largest error was with the ammonia partial pressure measurement, this variable was the dependent variable. Solving Eq. (5) for P_{NH_3} and expressing the forward rate constant in Arrhenius form, the following is obtained:

$$P_{NH_3} = [(N_s/F_0)A_0' \exp\{-E_a/RT\} (2m + 1)P_t]^{1/(2m+1)}. \quad (6)$$

A_0' and E_a are the preexponential factor and apparent activation energy, respectively. Experimentally determined values of ammonia partial pressure, molar flow rate, and temperature provided the input data for the statistical procedure which performed a nonlinear least-squares regression analysis. A Gauss–Newton method was used by the statistical procedure to achieve convergence. The output from the analysis consisted of the kinetic parameters A_0', E_a, and m. The value of N_s was determined either directly from the CO chemisorption measurement or from a model (discussed further below) which accounts for the gradual disappearance of active catalyst sites by particle ripening. It is later shown that the latter approach more accurately predicts the value of N_s corresponding to each ammonia partial pressure measurement. After the kinetic parameters were determined, the ammonia synthesis turnover frequency was calculated using Eq. (2) at 673 K, 5 Pa ammonia partial pressure. This allowed comparison of turnover frequencies at the same temperature and ammonia partial pressure for the different catalysts, and allowed comparison with other data reported at these conditions in the literature (*2, 10*).

Ammonia Synthesis Kinetics Measurements

Figure 2 shows the reactor effluent ammonia partial pressure vs molar flow rate at several temperatures for a 7.2% Fe/TiO_2 catalyst. The curves represent the least-squares fit of the kinetic model (Eq. (6)) to the entire data set. It should be noted that the temperatures listed in the caption of Fig. 2 are in the same chronological order in which they were encountered during the experiment. Examining the agreement between the curves derived from fit of the kinetic model and the experimentally measured points, an interesting trend is observed. All measured ammonia partial pressures at 682 K are above the model curve. The measured values at 673 K agree closely with the kinetic model fit, and the ammonia partial pressures measured at 662 and 693 K are all less than the model-determined values. This phenomenon reflects the fact that the data were collected over a slowly deactivating catalyst. At the temperatures of the experiment the catalyst particles were becoming enlarged due to Ostwald ripening (*36*). This gradual coarsening or enlarging of the particles causes a slow loss of active catalyst surface area. Thus, the value of N_s

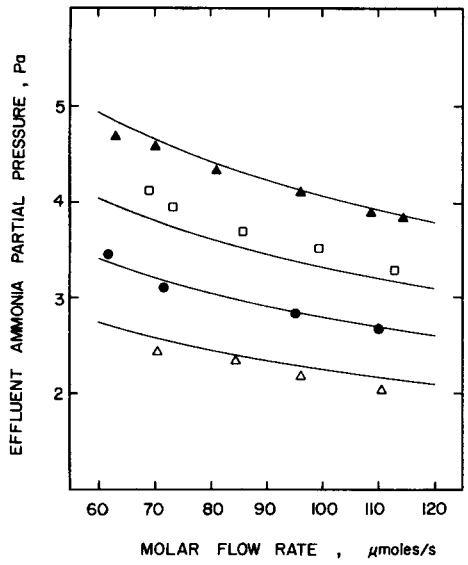

FIG. 2. Effluent ammonia partial pressure vs molar flow rate for 7.2% Fe/TiO_2 catalyst: (□) 682 K; (●) 673 K; (△) 662 K; (▲) 693 K. Curves indicate fit of the kinetic model (Eq. (6)) to the data.

measured at the end of each ammonia synthesis kinetics measurement does not represent the true number of active catalyst sites corresponding to each ammonia partial pressure measurement. Since this phenomenon is not accounted for in the kinetic model, the model is inadequate. X-ray diffraction results are presented below which indicate that the particles become significantly larger during the ammonia synthesis kinetics measurement.

Because of the high ratio of surface to bulk atoms, small catalyst particles have a high degree of surface free energy. At high temperatures small particles tend to become enlarged to reduce this surface free energy. Growth of catalyst particles while measuring the reaction kinetics over supported metal catalysts is often unavoidable since catalyst particle growth rates are often significant at the temperatures of interest for many catalytic reactions. To obtain kinetic parameters which represent the intrinsic kinetics at the catalyst surface, the model must account for the gradual loss of catalyst sites which occurs during the ammonia synthesis kinetics measurement. In what follows, a model is developed and used to predict values of N_s at various times during the ammonia synthesis kinetics measurement to account for the gradual disappearance of active catalyst sites. It is shown that such a kinetic model which accounts for deactivation of the catalyst better represents the data. As a result, the kinetic parameters extracted from the data using the modified model better represent the actual values.

Expressions describing the kinetics of particle growth in supported catalysts have been developed and discussed in the literature (*36–41*). Generally, these expressions have the form

$$\langle d\rangle^n = \langle d_0\rangle^n + k_{pg}t, \tag{7}$$

where $\langle d_0\rangle$ is the average catalyst particle diameter at time zero and $\langle d\rangle$ is the average particle diameter after time t. The rate constant for particle growth, k_{pg}, can be expressed in Arrhenius form, i.e., $k_{pg} = A_{pg}\exp\{-E_{a,pg}/RT\}$, where A_{pg} and $E_{a,pg}$ are the preexponential factor and apparent activation energy for particle growth, respectively. Values of n are typically in the range 1–7, depending on the mechanism of the particle growth process (*38*).

If a catalyst particle maintains its geometry during growth, its surface-average diameter is inversely proportional to the number of surface metal atoms

$$\langle d_s\rangle = c\frac{N_t}{N_s}, \tag{8}$$

where c is a constant which depends on the particle geometry and other constants (*42*) and N_s is the number of surface metal atoms. N_t is the total number of metal atoms in the catalyst. Substituting Eq. (8) into Eq. (7) provides an expression for the time-dependent number of surface metal atoms in terms of the initial number of surface metal atoms, $N_{s,0}$,

$$\frac{1}{N_s^n} = \frac{1}{N_{s,0}^n} + k'_{pg}t = \frac{1}{N_{s,0}^n} + A'_{pg}\exp\{-E_{a,pg}/RT\}t, \tag{9}$$

where $k'_{pg} = k_{pg}/(cN_t)^n$ and $A'_{pg} = A_{pg}/(cN_t)^n$. Over the course of the ammonia synthesis kinetics measurements in this study, the catalyst was exposed to several temperatures. For a catalyst exposed to M temperatures for a time t_i at each temperature T_i, the number of surface metal atoms, $N_{s,M}$, after time t_M at the Mth temperature is given as

$$\frac{1}{N_{s,M}^n} = \frac{1}{N_{s,0}^n} + A'_{pg}\left[\sum_{i=1}^{M-1}\exp\{-E_{a,pg}/RT_i\}t_i + \exp\{-E_{a,pg}/RT_M\}t_M\right]. \tag{10}$$

This expression allows calculation of the number of surface metal atoms at any time, $t = \sum_{i=1}^{M-1} t_i + t_M$, in terms of the initial number of surface metal atoms for a catalyst exposed to more than a single temperature.

In this investigation the CO chemisorption measurement was performed at the end

of the ammonia synthesis kinetics measurement; thus $N_{s,0}$ is unknown. Expressing Eq. (10) as the number of surface metal atoms at the end of the ammonia synthesis kinetics measurement, N_{s,M_f}, in terms of the initial number of surface metal atoms, the following is obtained:

$$\frac{1}{N^n_{s,M_f}} = \frac{1}{N^n_{s,0}} + A'_{pg} \sum_{i=1}^{M_f} \exp\{-E_{a,pg}/RT_i\} t_i. \quad (11)$$

Eliminating $N_{s,0}$ from Eq. (10) using Eq. (11) yields the following expression, which describes the number of surface metal atoms at time t_M and temperature T_M, in terms of the number of surface metal atoms at the end of the ammonia synthesis kinetics measurement,

$$\frac{1}{N^n_{s,M}} = \frac{1}{N^n_{s,M_f}} + A'_{pg} \left[\exp\{-E_{a,pg}/RT_M\} t_M - \sum_{i=M}^{M_f} \exp\{-E_{a,pg}/RT_i\} t_i \right]. \quad (12)$$

N_{s,M_f} is the number of surface metal atoms determined from CO chemisorption. Solving for $N_{s,M}$ and substituting this into the kinetic model (Eq. (6)) provides a kinetic model which accounts for the gradual disappearance of surface metal atoms, or active catalyst sites. In what follows, we refer to Eq. (12) as the catalyst site disappearance (CSD) model. After incorporating the CSD model into the kinetic model, the input data required to extract the kinetic parameters from the data consisted of ammonia partial pressure, molar flow rate, temperature, number of active catalyst sites from CO chemisorption, and the time from the start of the ammonia synthesis kinetics measurement corresponding to the particular ammonia partial pressure measurement. Since particle growth kinetic parameters n, $E_{a,pg}$, and A'_{pg} are included in the model, analysis of the data is capable of yielding information about the particle growth kinetics. For the purpose of this investigation we found it more appropriate to constrain n and $E_{a,pg}$ to the same values for each catalyst investigated. Below it is shown how adequate estimates of these parameters can be determined from existing literature data.

There are two mechanisms by which supported catalyst particles become enlarged. The first of these involves growth by migration, collision, and coalescence of particles on the support surface (*40, 41*). An atom diffusing on a particle surface will migrate to one side of the particle causing the particle to advance a distance of one atomic diameter. As this happens repeatedly, the net effect is a Brownian-type migration of the particle on the support surface. When this migrating particle collides with another particle, the two will coalesce to form one particle. In a system where this occurs, the rate of particle growth is controlled either by migration of the particle on the support surface or by coalescence of the particles. It has been shown that particle growth by this process is insignificant for particles larger than about 5 nm (*36*). Since the catalyst particles in the present investigation are larger than 20 nm it was justified to neglect this mechanism of particle growth.

The second mechanism for particle growth is by Ostwald ripening. Ostwald ripening involves migration of individual atoms which become dislodged from particle edges and migrate randomly over the support surface. These migrating atoms collide with and attach to other particles. This leads to growth of large particles at the expense of smaller particles. Ostwald ripening rates are controlled either by diffusion of atoms over the support surface, or by dissociation of atoms from particle edges. For particle growth rates controlled by surface diffusion, n is 4; whereas for rates controlled by edge dissociation, n is 3. Wynblatt and Gjostein (*36*) who have developed theoretical expressions for catalyst particle growth rates by this mechanism, argue that surface diffusion is the controlling particle growth mechanism except for "very small particles." No quantitative value for this statement was given.

However, the iron particles in this study were larger than those typical for most supported catalysts; thus it is probable that diffusion of atoms on the support was the controlling particle growth mechanism. Thus, n was given the value 4.

Wynblatt and Gjostein (*36*) have shown that when particle growth rate is controlled by surface diffusion, the particle growth apparent activation energy is given by

$$E_{a,pg} = H_s^m + \Delta H_{ps}, \qquad (13)$$

where

$$\Delta H_{ps} = H_p - H_s. \qquad (14)$$

H_s^m is the energy barrier for migration of an atom on the support to an adjacent site. H_p is the energy for dissociation of an atom from the particle surface, and H_s is the binding energy of an atom to the support surface. It has been shown that H_s^m is approximately related to H_s by the relation (*36*)

$$H_s^m = 0.1H_s. \qquad (15)$$

Combination of Eqs. (13)–(15) yields

$$E_{a,pg} = H_p - 0.9H_s. \qquad (16)$$

The binding energy of an atom to the support surface can be determined from the contact angle between the metal particle and the oxide surface. The work of adhesion, W_{adh}, of a liquid drop or solid particle in contact with a surface is given as

$$W_{adh} = \gamma_{M-V}(1 + \cos\theta), \qquad (17)$$

where θ is the contact angle and γ_{M-V} is the metal-vapor interfacial energy. Determination of these values, along with the area occupied by a single atom allows calculation of the binding energy of an atom to the oxide surface. Kingery (*43, 44*) and Humenik and Kingery (*45*) have determined contact angles and metal-vapor interfacial energies for drops of molten iron, nickel, and silicon on various oxides. Using their data for drops of iron on a titania substrate in a hydrogen environment, a work of adhesion of 900 ergs cm^{-2} was determined. Using this value and the area occupied by a single iron atom (*28*) the binding energy was calculated to be 33 kJ $mole^{-1}$. Work of adhesion values for small solid iron particles on α-alumina determined by Pilliar and Nutting (*46*) agree closely with the liquid values determined by Humenik and Kingery (*45*) for the same system, suggesting that work of adhesion for liquid and solid is not greatly different. To calculate the particle growth apparent activation energy from Eq. (16), the energy for dissociation of an iron atom from the particle surface is needed. Wynblatt and Gjostein (*36*) have suggested that this value is close to the sublimation energy, which for iron (*47*) is 415 kJ $mole^{-1}$. From Eq. (16), the particle growth apparent activation energy is calculated to be 385 kJ $mole^{-1}$. This value is within the range of measured particle growth apparent activation energies for several supported catalyst systems compiled by Wanke and Flynn (*37*) from many literature sources, and is thus considered to be reasonable. This was the value used in the CSD model in this investigation.

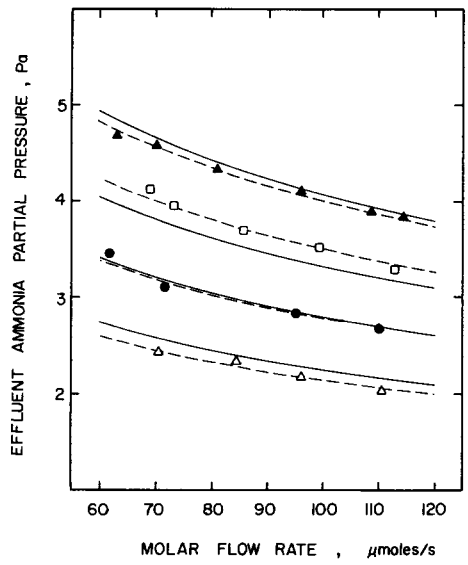

FIG. 3. Effluent ammonia partial pressure vs molar flow rate for 7.2% Fe/TiO_2 catalyst: (□) 682 K; (●) 673 K; (△) 662 K; (▲) 693 K. Solid curves indicate fit of the kinetic model assuming constant number of catalyst sites; dashed curves indicate fit of the kinetic model with the CSD model included in the kinetic model.

Figure 3 shows measured ammonia partial

TABLE 1

Kinetic Parameters, Turnover Frequency, and MSD for 7.2% Fe/TiO_2 Catalyst

	A_0' Preexponential factor ($Pa^{2m} \cdot ks^{-1}$)	E_a Apparent activation energy ($kJ \cdot mole^{-1}$)	m Ammonia partial pressure dependence	A_{pg}' Particle growth preexponential factor ($\mu mole^{-4} \cdot ks^{-1}$)	r_{NH_3} Ammonia synthesis turnover frequency (ks^{-1})	Mean square deviation
Constant N_s	$(2.3 \pm 21.6) \times 10^{13}$	188.9 ± 49.9	0.79 ± 0.32	—	0.004	0.0201
N_s predicted by CSD model	$(2.4 \pm 12.8) \times 10^{16}$	229.1 ± 22.3	0.84 ± 0.12	$(4.12 \pm 0.04) \times 10^{18}$	0.003	0.0025

pressure vs flow rate for the above-discussed 7.2% Fe/TiO_2 catalyst. The dashed curves represent the fit of the kinetic model to the data after incorporating the CSD model into the kinetic model. The solid curves, which show the fit of the kinetic model which does not include the CSD model, are included for comparison. Agreement between the measured values and the model has clearly improved. Table 1 shows values of the kinetic parameters and their associated 95% confidence interval extracted from the data for constant N_s, and for N_s predicted by the CSD model. Note that after incorporating the CSD model into the kinetic model, the 95% confidence interval for each parameter was significantly reduced, indicating improvement in the precision of the kinetic parameter estimation. Values of the kinetic parameters extracted from the data and turnover frequency determined using the model which includes the CSD model are different than the values extracted from the data using the model which does not include the CSD model. The value for the particle growth preexponential factor extracted from the data is included in Table 1. Also shown in Table 1 are the mean square deviations (MSD) obtained from the regression analyses. After incorporating the CSD model into the kinetic model the MSD was reduced by nearly an order of magnitude, indicating better agreement between the model and the data. It should be noted that the additional adjustable parameter will improve the agreement between the model and the data regardless of the statistical significance of the added parameter. However, below it will be shown that the additional adjustable parameter is statistically significant.

Figure 4 shows measured ammonia partial pressure vs flow rate at several temperatures for a hydrazine-pretreated 7.4%

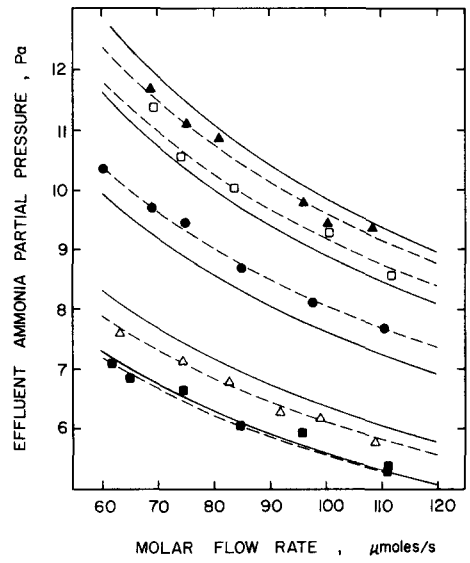

FIG. 4. Effluent ammonia partial pressure vs molar flow rate for 7.4% hydrazine-pretreated Fe/TiO_2 catalyst: (●) 673 K; (■) 656 K; (□) 682 K; (△) 663 K; (▲) 688 K. Solid curves indicate fit of the kinetic model assuming constant number of catalyst sites; dashed curves indicate fit of the kinetic model with the CSD model included in the kinetic model.

TABLE 2

Kinetic Parameters, Turnover Frequency, and MSD for Hydrazine-Pretreated 7.4% Fe/TiO_2 Catalyst

	A'_0 Preexponential factor ($Pa^{2m} \cdot ks^{-1}$)	E_a Apparent activation energy ($kJ \cdot mole^{-1}$)	m Ammonia partial pressure dependence	A'_{pg} Particle growth preexponential factor ($\mu mole^{-4} \cdot ks^{-1}$)	r_{NH_3} Ammonia synthesis turnover frequency (ks^{-1})	Mean square deviation
Constant N_s	$(1.4 \pm 5.6) \times 10^9$	126.4 ± 20.8	0.45 ± 0.15	—	0.049	0.1190
N_s predicted by CSD model	$(1.7 \pm 2.6) \times 10^{11}$	153.4 ± 8.1	0.50 ± 0.05	$(4.04 \pm 0.26) \times 10^{18}$	0.041	0.0098

Fe/TiO_2 catalyst. The solid curves represent the fit of the kinetic model with N_s held constant at the value determined from CO chemisorption. Again, the temperatures listed in the caption are in the same chronological order as were run in the ammonia synthesis kinetics measurement. Ammonia partial pressures measured at 673 K are well above those calculated from the kinetic model. Measured ammonia partial pressures at 656 K agree closely with those calculated from the model, whereas the measured values at 682 K are all higher than those determined by the model. Ammonia partial pressures measured at 663 and 688 K are lower than the model-calculated values. Generally, ammonia partial pressures measured early in the ammonia synthesis kinetics measurement are higher than those predicted by the model, while as time progresses, the number of active catalyst sites decreases due to particle ripening, and eventually, measured ammonia partial pressures become lower than the model-calculated values.

After incorporating the CSD model into the kinetic model the dashed curves in Fig. 4 were obtained. Better agreement between the measured and calculated values is clearly the case. Shown in Table 2 are the kinetic parameters, turnover frequency, and the MSD obtained both before and after incorporating the CSD model into the kinetic model. A significant reduction in the 95% confidence interval for each kinetic parameter was observed. As with the above-discussed 7.2% Fe/TiO_2 catalyst which was not pretreated with hydrazine, the values of the kinetic parameters and turnover frequency changed after the CSD model was incorporated into the kinetic model. Also, the MSD was reduced by more than one order of magnitude. The ammonia synthesis turnover frequency is slightly more than one order of magnitude greater than that of the 7.2% Fe/TiO_2 catalyst not pretreated with hydrazine (Table 1). The apparent activation energy and ammonia partial pressure dependence are significantly lower than the values obtained for the 7.2% Fe/TiO_2 catalyst not pretreated with hydrazine.

Figure 5 shows ammonia partial pressure vs flow rate at several temperatures for a hydrazine-pretreated K-promoted 7.0% Fe/TiO_2 catalyst. The solid curves represent the fit of the kinetic model with the number of catalyst sites constant and equal to the value determined from CO chemisorption. Again, the same trend is apparent regarding gradual loss of catalyst sites. Ammonia partial pressures measured early in the ammonia synthesis kinetics measurement are generally greater than those predicted by the model, while ammonia partial pressures measured near the end of the ammonia synthesis kinetics measurement generally fall below the

TABLE 3

Kinetic Parameters, Turnover Frequency, and MSD for Hydrazine-Pretreated K-Promoted 7.0% Fe/TiO_2 Catalyst

	A'_0 Preexponential factor ($Pa^{2m} \cdot ks^{-1}$)	E_a Apparent activation energy ($kJ \cdot mole^{-1}$)	m Ammonia partial pressure dependence	A'_{pg} Particle growth preexponential factor ($\mu mole^{-4} \cdot ks^{-1}$)	r_{NH_3} Ammonia synthesis turnover frequency (ks^{-1})	Mean square deviation
Constant N_s	$(7.0 \pm 25.5) \times 10^7$	107.2 ± 19.2	0.32 ± 0.14	—	0.118	0.1184
N_s predicted by CSD model	$(7.0 \pm 20.5) \times 10^8$	120.7 ± 15.6	0.34 ± 0.10	$(3.69 \pm 0.96) \times 10^{21}$	0.102	0.0413

model predictions. The trend here is not as apparent as with the above unpromoted catalysts.

The dashed curves in Fig. 5 represent the fit obtained after incorporating the catalyst site disappearance model into the kinetic model. Agreement between the measured and calculated values has improved. Table 3 shows the kinetic parameters obtained for this catalyst. As with the above-discussed catalysts, the 95% confidence intervals were reduced after incorporating the CSD model into the kinetic model. Also, the values of the parameters are different than those determined without the CSD model included in the kinetic model. Reduction of the confidence intervals with this catalyst is not as pronounced as with the unpromoted catalysts. Reduction of the MSD after incorporating the CSD model into the kinetic model was by slightly less than a factor of three. This is less than the tenfold decrease seen with the unpromoted catalysts. The apparent activation energy and ammonia partial pressure dependence have decreased relative to those of the unpromoted 7.4% Fe/TiO_2 hydrazine-pretreated catalyst. The turnover frequency has increased by slightly less than a factor of 2.5 over the unpromoted 7.4% Fe/TiO_2 hydrazine-pretreated catalyst.

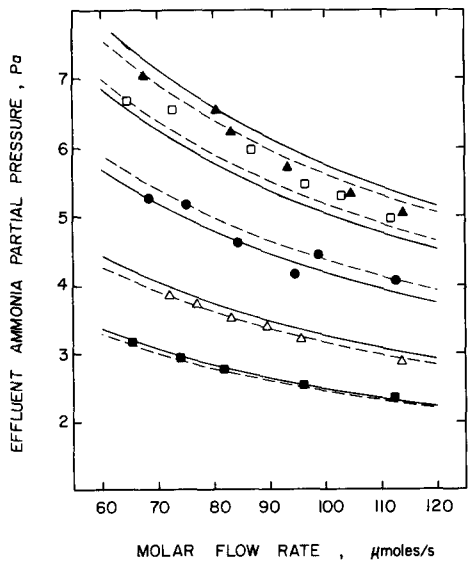

FIG. 5. Effluent ammonia partial pressure vs molar flow rate for hydrazine-pretreated K-promoted 7.0% Fe/TiO_2 catalyst: (●) 673 K; (■) 644 K; (□) 684 K; (△) 659 K; (▲) 692 K. Solid curves indicate fit of the kinetic model assuming constant number of catalyst sites; dashed curves indicate fit of the kinetic model with the CSD model included in the kinetic model.

Figure 6 shows ammonia partial pressure vs flow rate at several temperatures for a hydrazine-pretreated Cs-promoted 6.7% Fe/TiO_2 catalyst. The solid curves represent the fit of the data when N_s was held constant

TABLE 4

Kinetic Parameters, Turnover Frequency, and MSD for Hydrazine-Pretreated Cs-Promoted 6.7% Fe/TiO_2 Catalyst

	A'_0 Preexponential factor ($Pa^{2m} \cdot ks^{-1}$)	E_a Apparent activation energy ($kJ \cdot mole^{-1}$)	m Ammonia partial pressure dependence	A'_{pg} Particle growth preexponential factor ($\mu mole^{-4} \cdot ks^{-1}$)	r_{NH_3} Ammonia synthesis turnover frequency (ks^{-1})	Mean square deviation
Constant N_s	$(2.9 \pm 23.4) \times 10^9$	129.2 ± 43.8	0.26 ± 0.22	—	0.115	0.0507
N_s predicted by CSD model	$(1.8 \pm 10.2) \times 10^9$	126.3 ± 29.6	0.39 ± 0.18	$(1.01 \pm 0.19) \times 10^{22}$	0.082	0.0234

in the kinetic model. The dashed curves represent the fit when the CSD model was included in the kinetic model. Again, agreement between the model and the data improved after the CSD model was included in the kinetic model. Table 4 contains values of the kinetic parameters extracted from the data. As with the K-promoted catalyst, the 95% confidence intervals and MSD were reduced, but not as much as with the unpromoted catalysts. Also, the values of the kinetic parameters have changed relative to those determined before incorporating the CSD model into the kinetic model. The apparent activation energy and ammonia partial pressure dependence are slightly larger than those observed for the K-promoted catalyst. The turnover frequency for the Cs-promoted catalyst is slightly less than that of the K-promoted catalyst.

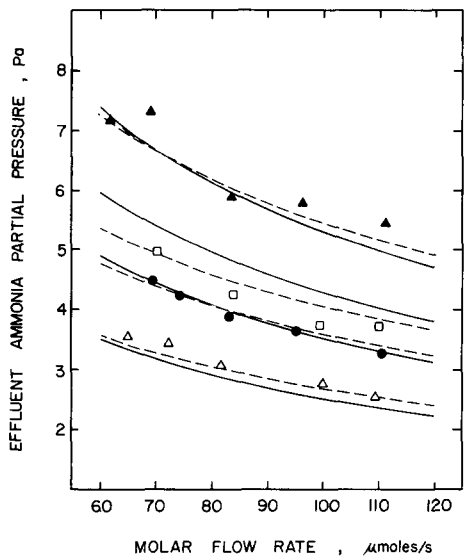

FIG. 6. Effluent ammonia partial pressure vs molar flow rate for hydrazine-pretreated Cs-promoted 6.7% Fe/TiO_2 catalyst: (▲) 685 K; (●) 666 K; (△) 652 K; (□) 675 K. Solid curves indicate fit of the kinetic model assuming constant number of catalyst sites; dashed curves indicate fit of the kinetic model with the CSD model included in the kinetic model.

Table 5 shows BET surface area, CO uptake, and iron particle sizes for each of the catalysts studied. The surface-average particle size was determined from the CO uptake, and the volume-average particle size was determined by X-ray diffraction line-broadening. The particle sizes determined by the two methods for the unpromoted catalysts are in good agreement. For the unpromoted catalysts, the CO uptake for the hydrazine-pretreated catalyst is slightly higher than that of the unpretreated catalyst, whereas the particle sizes determined from X-ray diffraction have close to the same value. The lower CO uptake on the promoted catalysts and the large difference between the surface and volume-average particle sizes most likely indicates that the iron surface is covered by the alkali metal promoter. The volume-average particle size for

TABLE 5

BET Surface Area, CO Uptake, Dispersion, and Particle Sizes for Fe/TiO_2 and Alkali-Promoted Fe/TiO_2 Catalysts

Catalyst	BET surface area	CO uptake (μmole · g^{-1})	D	$\langle d_s \rangle$ (nm)	$\langle d_v \rangle$ (nm)
7.2% Fe/TiO_2	—	16.5	0.0256	35.1	46.4
7.4% Fe/TiO_2 hydrazine-pretreated	45.6 ± 0.4	18.4	0.0343	32.4	46.6
7.0% Fe/TiO_2 hydrazine-pretreated K-promoted	46.0 ± 0.4	2.9	0.0046	194.5	—
6.7% Fe/TiO_2 hydrazine-pretreated Cs-promoted	46.5 ± 0.4	3.2	0.0053	168.7	31.4

the Cs-promoted catalyst is significantly smaller than those of the unpromoted catalysts. The BET surface areas of all the catalysts agree closely with the value of 47.2 m^2 g^{-1} (determined elsewhere (*18*)) for a catalyst before kinetic measurements, indicating that the support has not undergone any significant morphological changes during the ammonia synthesis kinetics measurements.

DISCUSSION

For each of the above-discussed catalysts, significant reductions in the MSD and the 95% confidence intervals of the kinetic parameters were achieved by modifying the kinetic model to account for gradual disappearance of catalyst sites by Ostwald ripening of supported particles. Also, the values of the kinetic parameters extracted from the data using the modified form of the model were different from those extracted from the data using the kinetic model which does not account for deactivation of the catalyst. The modified form of the kinetic model was obtained by incorporating the CSD model into the kinetic model. This increased by one the number of adjustable parameters in the kinetic model. Obviously, an increase in the number of adjustable parameters in the model will result in an improved fit regardless of whether the model better represents the data. Therefore, before concluding that the modified kinetic model better represents the data, it must be ascertained that addition of the CSD model to the kinetic model is statistically significant. Statistical significance of the CSD model was verified by applying the F-statistical test. Accordingly, the F-statistic between the kinetic model with and without the CSD model was calculated using information obtained from the regression analysis for each case. Table 6 shows values of the F-statistic for each of the catalysts studied. Also shown in the table are the minimum values of the F-statistic required for statistical significance at the 99.9% confidence level (*48*). The F-statistic values are well above the minimum values required for statistical significance at the 99.9% confidence level, indicating that the modification to the kinetic model to account for deactivation of the supported particles during the ammonia synthesis kinetics measurement is statistically significant.

Since the modified form of the kinetic model was verified to be statistically more representative of the data, it follows that the kinetic parameters extracted from the data using this model better represent the true values. Thus, accounting for deactivation of the catalyst improved the accuracy of the kinetic parameters extracted from the data. In addition, because of the decrease of the

TABLE 6

Statistical Significance of Incorporating the CSD Model into the Kinetic Model

Catalyst	*F*-statistic between kinetic model with and without CSD model	Required *F*-statistic for significance at the 99.9% confidence level
7.2% Fe/TiO_2	112	17
7.4% Fe/TiO_2 hydrazine-pretreated	300	14
7.0% Fe/TiO_2 hydrazine-pretreated K-promoted	31	14
6.7% Fe/TiO_2 hydrazine-pretreated Cs-promoted	31	17

95% confidence intervals, the values of the kinetic parameters extracted from the data using the modified model are more precise. Inherent in this argument is the implication that if deactivation of a catalyst occurs during kinetics measurements and is not accounted for, this can obscure the true values and introduce additional uncertainty to the kinetic parameters. Consider for example the preexponential factor for the 7.2% Fe/TiO_2 catalyst (Table 1). Accounting for deactivation of the catalyst resulted in a change in the value by 3 orders of magnitude. This illustrates how substantial error to the kinetic parameters can result from catalyst deactivation effects. Since the kinetic parameters extracted from the data using the modified kinetic model better represent the true values, further discussion of the kinetic parameters refers to those obtained using the model which accounts for deactivation of the catalysts.

Due to the high activation energy associated with the deactivation process, running the reaction at the highest temperature for an extended period would likely eliminate this effect. However, for deactivation processes with lower, or no temperature dependence, this would not always be possible.

The data from the ammonia synthesis kinetics measurements was also analyzed using the CSD model with the exponent, n, having a value of 3 instead of 4 (*22*). For the unpromoted catalysts, the MSDs for $n = 3$ and $n = 4$ were essentially the same. The MSDs for the promoted catalysts were slightly lower for $n = 3$, but the differences were minor, and it is felt that there is insufficient justification to claim that $n = 3$ is the more appropriate value. Since a rate process governed by diffusion of atoms over the support surface ($n = 4$) is expected for particles as large as those in this study, it is felt that $n = 4$ is the appropriate value for the exponent in the CSD model.

Since the preexponential factor for the particle growth process was obtained from analysis of the data with the CSD model incorporated in the kinetic model (Tables 1–4), Eq. (12) can be used to predict the number of catalyst sites at various times during the ammonia synthesis kinetics measurements. Table 7 shows values of CO uptake calculated from Eq. (12) for each catalyst after hydrogen reduction of the catalyst and before the 75% H_2, 25% N_2 mixture was introduced. The surface-average particle size calculated from this CO uptake is also shown for the unpromoted catalysts. CO uptakes measured after the ammonia synthesis kinetics measurement were shown in Table 5. The CO uptakes calculated at the begin-

TABLE 7

Carbon Monoxide Uptake and Surface-Average Particle Size at the Beginning of the Ammonia Synthesis Kinetics Measurement Calculated from the CSD Model

Catalyst	CO uptake (μmole · g^{-1})	$\langle d_s \rangle$ (nm)	$\langle d_v \rangle$ (nm)
7.2% Fe/TiO_2	24.3	23.9	—
7.4% Fe/TiO_2 hydrazine-pretreated	24.8	24.0	—
7.0% Fe/TiO_2 hydrazine-pretreated K-promoted	4.7	—	—
6.7% Fe/TiO_2 hydrazine-pretreated Cs-promoted	3.7	—	—
6.3% Fe/TiO_2 reduced 24 h H_2 at 673 K[a]	26.2[b]	21.3	29.2
	25.9[b]	21.6	26.5
6.3% Fe/TiO_2 reduced 24 h H_2 at 723 K[a]	17.9[b]	31.2	33.1

[a] Taken from Ref. (*18*).
[b] Measured value.

ning of the ammonia synthesis kinetics measurement (immediately after hydrogen reduction) for the unpromoted catalysts agree closely with CO uptakes measured previously by us (also listed in Table 7) in detailed characterization of similar Fe/TiO_2 catalysts (*18*). The catalysts in Ref. (*18*) were reduced for the same time, but at a slightly lower temperature (673 K) and higher temperature (723 K). It is reasonable that the particle size estimated from the calculated CO uptake for the 693 K-reduced catalysts of the present study are between the particle sizes for catalysts reduced at lower and higher temperatures. This result confirms the correctness of the CSD model, since reasonable values of CO uptake are obtained when projected to earlier times.

Other catalyst deactivation mechanisms, such as poisoning, can be ruled out by examining the X-ray diffraction particle sizes at the end of the ammonia synthesis kinetics measurement for the unpromoted catalysts (Table 5), and comparing these with X-ray diffraction particle sizes measured after the reduction step for similar catalysts characterized by us in a previous study (*18*). Table 7 shows volume-average particle size determined from X-ray diffraction after the 24 h reduction step for catalysts reduced at 673 and 723 K. The catalysts in the present investigation were reduced at 693 K; thus, the particle sizes for the catalysts reduced at 673 and 723 K represent what should be upper and lower limits for the particles of the 693 K-reduced catalyst before introduction of the 25% N_2, 75% H_2 mixture. The X-ray diffraction particle sizes of 46.4 nm and 46.6 nm for the unpromoted catalysts (Table 5) are significantly larger than the expected values at the beginning of the ammonia synthesis kinetics measurement, indicating that the particles must have grown during the ammonia synthesis kinetics measurement.

Comparing the kinetic parameters obtained for the 7.2% Fe/TiO_2 and hydrazine-pretreated 7.4% Fe/TiO_2 catalysts shown in Tables 1 and 2, respectively, some differences are noted. The apparent activation energy and ammonia partial pressure dependence for the hydrazine-pretreated catalyst are lower than those of the catalyst not pretreated with hydrazine. The value of 0.5 for the ammonia partial pressure dependence for the hydrazine-pretreated catalyst is closer to the values reported by others for clean iron surfaces (*29–32*). The turnover frequency for the hydrazine-pretreated catalyst is about 1 order of magnitude higher than that of the unpretreated catalyst. Turnover frequencies for these catalysts agree well with turnover frequencies measured by Santos *et al.* (*10*) for similar Fe/TiO_2 catalysts. Turnover frequencies for Fe/TiO_2 are about 4 orders of magnitude lower than those reported for Fe/MgO catalysts (*2*) and are about 5 orders of magnitude lower than the turnover frequency reported for an Fe/SiO_2 catalyst (*10*).

Characterization data presented in Table 5 show higher dispersion for the hydrazine-pretreated catalyst vs the catalyst not pretreated with hydrazine. The particle sizes measured by X-ray diffraction line-broaden-

ing are nearly the same for the two catalysts. Similar X-ray diffraction particle size along with higher dispersion suggests higher degreee of particle surface poisoning with the catalyst not pretreated with hydrazine. These differences in the kinetic parameters, turnover frequency, and degree of surface poisoning between the unpretreated and hydrazine-pretreated catalysts suggest that the surfaces of these two catalysts are different.

When considering the catalytic properties of titania-supported metals, one must consider that the surfaces of the supported particles are influenced by a strong metal-support interaction (SMSI). This effect is responsible for drastic reduction in capacity to chemisorb H_2 and CO when reduced at temperatures higher than about 770 K. The SMSI effect was first observed by Tauster *et al.* (*49*) and Tauster and Fung (*50*) and has been well-studied by many other investigators. Earlier works (*49–56*) indicated that SMSI was due to electronic modification of supported particles by the reduced underlying support. However, Simoens *et al.* (*57*) and others (*10, 18, 58–61*) have shown that the surfaces of metals supported on titania are contaminated with a titania suboxide species which migrates to the particle surfaces during reduction. More recently, Raupp and Dumesic (*62*) showed that both electronic effects induced from the reduced underlying support and titania adspecies are present in the SMSI effect on titania-supported catalysts. Previous results from our laboratory (*18*) agree with results of others (*58*) which indicate that effects from migrating titania species on the particle surfaces can be detected at temperatures as low as 673 K. Since the catalysts in the present work were reduced at 693 K, some effects of SMSI are expected.

In an investigation of the ammonia synthesis kinetics over Fe/TiO_2, Santos *et al.* (*10*) showed that the ammonia synthesis kinetics are influenced by the SMSI effect. They showed that, as the reduction temperature (and thus the extent of SMSI) increased, the apparent activation energy and the ammonia partial pressure dependence increased. They reported turnover frequencies for Fe/TiO_2 which were much lower than those obtained over Fe/SiO_2 and Fe/MgO. These authors attributed the lower turnover frequencies and changed kinetic parameters to the presence of titania adspecies on the surfaces of the iron particles. Since the ammonia synthesis reaction requires a large ensemble of surface atoms, it was argued that slight contamination of the surface should have a large effect on the number of sites on which the ammonia synthesis can occur. Changes in the apparent activation energy and ammonia partial pressure dependence were attributed to electronic modification of the iron surface by adsorbed titania species.

The differences in turnover frequency, kinetic parameters, and degree of particle surface poisoning between the hydrazine-pretreated and unpretreated catalysts in the present investigation may be interpreted in terms of a smaller extent of SMSI with the hydrazine-pretreated catalyst. The kinetic parameter and turnover frequency changes are consistent with the above-discussed observations of Santos *et al.* (*10*). It thus appears that the hydrazine pretreatment modified the titania support in a manner which inhibited the SMSI effect.

Hydrazine has been observed by Littrell and Tatarchuk (*63*) to reduce the surfaces of transition metal oxides. Using *in situ* X-ray photoelectron spectroscopy they observed decreases in the surface oxygen/metal ratio for a range of first-row transition metal oxides. While these workers did not consider the reduction of titania by hydrazine, they observed rapid reduction of similarly stable oxides; thus it is probable that titania will be reduced by hydrazine. Reduction of the titania surface by hydrazine would likely proceed by removal of surface oxygen anions and creation of surface anionic oxygen vacancies, similar to the reduction of titania by hydrogen proposed by Herrmann and Pichat (*64*),

$$\tfrac{1}{2}N_2H_4 + 2O^{2-} \rightleftarrows H_2O + \tfrac{1}{2}N_2 + O^{2-} + V_{O^{2-}}, \quad (18)$$

where $V_{O^{2-}}$ represents a surface anionic vacancy with two trapped electrons. Creation of anionic vacancies could render the surface more reactive, allowing hydrazine to react and replace surface oxygen anions with surface nitrogen anions as

$$\tfrac{1}{2}N_2H_4 + V_{O^{2-}} + O^{2-} \rightleftarrows V_{O^{2-}} + N^{2-} + H_2O. \quad (19)$$

As the catalyst is heated to 693 K in hydrogen during reduction, some surface nitrogen would likely be removed from the surface as nitrogen or ammonia, but some surface nitrogen would probably participate in formation of structural titanium nitride, which would be present as small TiN crystallites in the support surface. Equations (18) and (19) have the net effect of converting titanium dioxide to titanium nitride as

$$N_2H_4 + TiO_2 \rightleftarrows 2H_2O + \tfrac{1}{2}N_2 + TiN. \quad (20)$$

The free-energy change for this reaction is favorable by about 42 kJ $mole^{-1}$ at room temperature. The increased quantity of titanium nitride and the reduced quantity of titanium dioxide on the support surface would likely reduce the probability of forming the titania species which migrates to the surfaces of titania-supported particles, thus inhibiting the onset of SMSI.

Addition of potassium and cesium to Fe/TiO_2 resulted in an increase in the ammonia synthesis turnover frequency. For both of the promoted catalysts, the apparent activation energy and ammonia partial pressure dependence are significantly lower than those of the unpromoted Fe/TiO_2 catalyst. Potassium is slightly more effective than cesium in promoting the ammonia synthesis reaction. This is opposite the trend observed by Aika *et al.* (*8*) who determined that for supported ruthenium catalysts promoted with Na, K, and Cs the catalytic activity for ammonia synthesis increases in the order of decreasing work function (Na < K < Cs). Another interesting difference between this work and that of Aika *et al.* (*8*) is that they observed much larger increases in ammonia synthesis activity after addition of the promoter than was the case in the present work. Emmett and Brunauer (*65*) observed an eightfold increase in turnover frequency when potassium oxide was added to iron ammonia synthesis catalyst. A smaller increase (factor of 2–3) in ammonia synthesis rate was observed in the present study after addition of alkali. This could be attributed to titanium-oxygen adspecies on the surfaces of the alkali-promoted particles. Adsorbed titanium–oxygen species may interact with alkali to reduce the effectiveness of the promoter. This might be similar to the interaction of adsorbed oxygen with alkali on model polycrystalline iron surfaces investigated by Paál *et al.* (*66*). They found that oxygen coadsorbed with alkali caused a large decrease in nitrogen adsorption rate. The decrease in nitrogen adsorption rate was consistent with the increase in surface work function, which they also measured. This effect was attributed to a chemical interaction between coadsorbed oxygen and alkali on the polycrystalline surface. Such an interaction would decrease the ability of alkali to transfer electrons to the iron surface since transfer of electron density to the iron surface is the essential function of the promoter. A similar interaction between adsorbed titanium–oxygen species and adsorbed alkali is possible with the catalysts in this investigation. Such an interaction would explain the observation that the promoter only caused a modest increase in ammonia synthesis rate. Studies of the interaction of alkali and alumina promoters in iron-based ammonia synthesis catalysts has provided evidence for association of alkali with an alumina phase on the iron surface (*67*, *68*). Indeed, it is possible that a similar interaction between iron and titania may be present in the alkali-promoted Fe/TiO_2 catalysts.

For the catalysts considered in this study, kinetic parameters in the Temkin–Pyzhev model were determined. The following development demonstrates how heats of nitrogen adsorption on the catalysts can be estimated from the kinetic parameters. The

estimated heats of adsorption provide some insight concerning the nature of the catalytically active phase. For the purpose of this development, the ammonia synthesis is assumed to proceed according to the following two-step mechanism (*4, 29*)

$$N_2 + 2^* \rightarrow 2N^* \quad (21)$$

$$2N^* + 3H_2 \rightleftarrows 2^* + 2NH_3, \quad (22)$$

where * represents an active catalyst site. It has been well established that the first step is the rate limiting step, while the second step is in equilibrium.

Temkin (*29*) has shown that the forward rate constant, k_f, in Eq. (1) is given as

$$k_f = k_{ads,N_2}(K_{0,N_2}K_2)^{-m}, \quad (23)$$

where K_{0,N_2} is the equilibrium constant for nitrogen adsorption on a nonuniform surface, and is given by (*69*)

$$K_{0,N_2} = \left(\frac{k_{ads,N_2}}{k_{des,N_2}}\right) \exp\{\Delta H^0_{ads,N_2}/RT\}. \quad (24)$$

$\Delta H^0_{ads,N_2}$ is the heat of nitrogen adsorption at zero surface coverage. The rate constants k_{ads,N_2} and k_{des,N_2} are for adsorption and desorption of nitrogen, respectively, from a nonuniform surface, and can be expressed in Arrhenius form as

$$k_{ads,N_2} = A_{ads,N_2}\left(\frac{RT}{\gamma}\right) \exp\{-E^0_{ads,N_2}/RT\} \quad (25)$$

$$k_{des,N_2} = A_{des,N_2}\left(\frac{RT}{\beta}\right) \exp\{-E^0_{des,N_2}/RT\}, \quad (26)$$

where A_{ads,N_2} and A_{des,N_2} are preexponential factors. E^0_{ads,N_2} and E^0_{des,N_2} are activation energies for nitrogen adsorption and desorption at zero surface coverage, respectively. The parameters γ and β define the distribution of adsorption and desorption activation energies, respectively, for a nonuniform surface. K_2 is the equilibrium constant for Eq. (22), which can be expressed as

$$K_2 = C_2 \exp\{\Delta H_2/RT\}, \quad (27)$$

where C_2 is a constant. ΔH_2 is the enthalpy change for Eq. (22), which can be expressed as the difference between the enthalpies of formation of the products and reactants

$$\Delta H_2 = 2\Delta H_{f,NH_3} - \Delta H^0_{ads,N_2}. \quad (28)$$

$\Delta H_{f,NH_3}$ is the heat of formation of ammonia (45.9 kJ mole^{-1}). Use of $\Delta H^0_{ads,N_2}$ as the enthalpy of formation for $2N^*$ is valid since the surface coverage of N^* is very small under ammonia synthesis conditions. Ertl (*7*) has made measurements of the N^* surface coverage for a stoichiometric mixture (at 583 K, 80 kPa) which was far from equilibrium (reverse reaction negligible). He found that the surface coverage is very low, and in fact, he stated that the surface under these conditions is "essentially nitrogen-free." Substituting Eqs. (24)–(28) into Eq. (23), and invoking the relation $\Delta H^0_{ads,N_2} = E^0_{des,N_2} - E^0_{ads,N_2}$, obtain

$$k_f = A_{ads,N_2}\left(\frac{RT}{\gamma}\right)\left(\frac{A_{des,N_2}}{A_{ads,N_2}}\right)^m\left(\frac{\beta}{\gamma}\right)^m\left(\frac{1}{C_2}\right) \times \exp\{-(E^0_{ads,N_2} + m\Delta H^0_{ads,N_2} + 2m\Delta H_{f,NH_3})\}. \quad (29)$$

Given that $k_f = A_0 \exp\{-E_a/RT\}$, it follows that

$$A_0 = A_{ads,N_2}\left(\frac{RT}{\gamma}\right)\left(\frac{A_{des,N_2}}{A_{ads,N_2}}\right)^m\left(\frac{\beta}{\gamma}\right)^m\left(\frac{1}{C_2}\right) \quad (30)$$

and

$$E_a = E^0_{ads,N_2} + m\Delta H^0_{ads,N_2} + 2m\Delta H_{f,NH_3}. \quad (31)$$

Equation (31) indicates that the ammonia synthesis apparent activation energy depends on the nitrogen adsorption heat. Previous work has found that the activation energy for nitrogen adsorption is typically in the range 0–30 kJ mole^{-1} for promoted and unpromoted iron (*7, 70*). Using an aver-

TABLE 8

Heats of Nitrogen Adsorption at Zero Coverage Calculated from Kinetic Parameters Obtained from Ammonia Synthesis Kinetics Measurements

Catalyst	$\Delta H_{ads,0}$ Heat of adsorption (kJ $mole^{-1}$)
7.2% Fe/TiO_2	163.1 ± 45.2
7.4% Fe/TiO_2 hydrazine-pretreated	184.2 ± 32.3
7.0% Fe/TiO_2 hydrazine-pretreated K-promoted	219.1 ± 104.7
6.7% Fe/TiO_2 hydrazine-pretreated Cs-promoted	193.6 ± 152.2

age value of 15 kJ $mole^{-1}$, the heat of nitrogen adsorption for each of the catalysts were calculated from Eq. (31), and are shown in Table 8. The heats of nitrogen adsorption for the unpromoted catalysts are slightly lower than the reported 198–228 kJ $mole^{-1}$ values for iron (*7, 70*). The higher nitrogen adsorption heat for the hydrazine-pretreated catalyst may be related to the smaller extent of SMSI with this catalyst. It is noted that the heat of nitrogen adsorption increases as alkali promoter is added. This is likely an effect induced by the promoter. The effect of the promoter on the adsorption heat of molecular nitrogen has been well studied, and is known to increase as promoter is added; however, the influence of promoters on the strength of the Fe–N bond for dissociatively adsorbed nitrogen is more difficult to determine, and literature values are not available. The result in Table 8 indicates that, as with associatively adsorbed nitrogen, promoter increases the Fe–N bond strength for dissociatively adsorbed nitrogen.

It is interesting that catalysts with higher activity have smaller ammonia partial pressure dependence (Tables 1–4). The ammonia partial pressure dependence, m, is the ratio γ/α, where γ is the proportionality constant defining the linear distribution of nitrogen adsorption activation energies for a nonuniform surface, and α is the constant which defines the linear distribution of nitrogen adsorption heat. If an increase in activity is produced by creation of a few active sites, such as in the vicinity of the alkali promoter on the particle surface, this would result in sites near alkali metal atoms on the particle surfaces which have high binding energies for nitrogen adsorption, while sites located relatively far from the alkali promoter would have similar characteristics as the unpromoted catalysts. This idea is reasonable, since Heskett (*71*) has shown that alkali promoters on transition metals exert the promoter effect over a relatively short range.

CO uptakes (Table 5) for the promoted catalysts are substantially smaller than those of the unpromoted catalysts. This is probably due to alkali metal covering a significant portion of the supported particle surfaces. Since the work of Emmett and Brunauer (*24*) in the late thirties, it has been known that alkali promoters in iron ammonia synthesis catalysts cover a major portion of the iron surface. A more recent investigation of alkali promoters in supported catalysts is consistent with our observation that the promoter covers supported particle surfaces (*72*). Covering of the particle surfaces with alkali is probably the reason for the smaller volume-average particle size (determined by X-ray diffraction) in the Cs-promoted catalyst (Table 5). In the promoted catalysts the number of surface iron atoms available for dissociation from particle edges is substantially less than with the unpromoted catalysts. Since particles become enlarged by dissociation of atoms from particle edges and subsequent migration of these atoms over the support surface, a decrease in the number of surface iron atoms would most likely decrease particle growth rate.

Additional evidence for slower particle growth in the promoted catalysts is provided by estimating rates of particle growth in the

TABLE 9

Surface Iron Atom Disappearance Rates

Catalyst	Surface iron atom disappearance rate at the beginning of the ammonia synthesis kinetics measurement (μmoles ks^{-1}) $\times 10^4$	Surface iron atom disapperance rate at the end of the ammonia synthesis kinetics measurement (μmoles ks^{-1}) $\times 10^4$
7.2% Fe/TiO_2	3.67	0.53
7.4% Fe/TIO_2 hydrazine-pretreated	3.99	0.90
7.0% Fe/TiO_2 hydrazine-pretreated K-promoted	0.89	0.08
6.7% Fe/TiO_2 hydrazine-pretreated Cs-promoted	0.74	0.36

catalysts. Differentiation of Eq. (9) provides an expression for the surface iron atom disappearance rate expressed as micromoles per ks,

$$-\frac{dN_s}{dt} = \frac{1}{n} A'_{pg} \exp\{-E_{a,pg}/RT\} N_s^{n+1}. \tag{32}$$

Table 9 shows surface iron atom disappearance rates for each catalyst calculated from Eq. (32), using the above-determined particle growth kinetic parameters. Shown are the rates evaluated at the beginning and end of the ammonia synthesis kinetics measurement. Surface iron atom disappearance rates for the unpromoted catalysts have similar values. This is reasonable given the similarity of the catalysts. Surface iron atom disappearance rates for the promoted catalysts are smaller than those of the unpromoted catalysts. This is consistent with the smaller particle size of the Cs-promoted catalyst measured by X-ray diffraction. Particle growth rates for the promoted catalysts are similar at the beginning of the ammonia synthesis kinetics measurement, but the particle growth rate of the K-promoted catalyst at the end of the ammonia synthesis kinetics measurement is smaller than that of the Cs-promoted catalyst. The probable reason for this is that the reaction was run for a longer time with the K-promoted catalyst than with the Cs-promoted catalyst.

Above it was noted that for the promoted catalysts, the reductions in MSD and confidence intervals as a result of incorporating the CSD model into the kinetic model to account for ripening of supported particles were not as pronounced as with the unpromoted catalysts. This is consistent with slower particle growth rates with the unpromoted catalysts.

CONCLUSIONS

Several features of the ammonia synthesis over Fe/TiO_2 catalysts pretreated with hydrazine and promoted with alkali were investigated. A modified form of the Temkin–Pyzhev model which accounts for deactivation of the catalyst by Ostwald ripening of the supported particles was used to correlate the data. Aside from improving the accuracy and precision of kinetic parameters, the modified kinetic model supplied useful information about the kinetics of the particle ripening process. Differences in the turnover frequencies, kinetic parameters and CO uptakes for Fe/TiO_2 and hydrazine-pretreated Fe/TiO_2 catalysts were consistent with a smaller extent of SMSI for the

hydrazine-pretreated catalyst. The smaller extent of SMSI appears to be due to reduction of the surface and subsequent formation of titanium nitride on the support surface. The alkali promoters K and Cs reduced the ammonia partial pressure dependence and the apparent activation energy, but only provided a modest increase in the turnover frequency for the ammonia synthesis reaction. The alkali promoters may be interacting with adsorbed titania species on the surfaces of the supported particles. A smaller X-ray diffraction particle size for the Cs-promoted catalyst and smaller particle growth rates for the promoted catalysts indicated that the alkali promoters stabilized the iron particles against growth by Ostwald ripening. The smaller particle growth rates for the promoted catalysts are probably due to a smaller number of surface-exposed iron atoms which results from partial covering of the particles by alkali.

ACKNOWLEDGMENT

One of us (A.N.) thanks the Carolina Eastman company for a graduate research fellowship.

REFERENCES

1. Boudart, M., Delbouile, A., Dumesic, J. A., Khammoma, S., and Topsøe, H., *J. Catal.* **37,** 486 (1975).
2. Dumesic, J. A., Topsøe, H., Khammouma, S., and Boudart, M., *J. Catal.* **37,** 503 (1975).
3. Dumesic, J. A., Topsøe, H., and Boudart, M., *J. Catal.* **37,** 513 (1974).
4. Boudart, M., and Djega-Mariadassou, G., "Kinetics of heterogeneous Catalytic Reactions," Princeton Univ. Press, Princeton, NJ, 1984.
5. Asscher, M., Carrazza, J., Khan, M. M., Lewis, K. B., and Somorjai, G. A., *J. Catal.* **98,** 277 (1986).
6. Spencer, N. D., Schoonmaker, R. C., and Somorjai, G. A., *J. Catal.* **74,** 129 (1984).
7. Ertl, G., *Catal. Rev. Sci. Eng.* **21**(2), 201 (1980).
8. Aika, K. I., Hori, H., and Ozaki, A., *J. Catal.* **27,** 424 (1972).
9. Sueiras, J. E., Homs, N., Ramirez de la Piscina, P., Gracia, M., and Fierro, J. L. G., *J. Catal.* **98,** 264 (1986).
10. Santos, J., Phillips, J., and Dumesic, J. A., *J. Catal.* **81,** 147 (1983).
11. Santos, J., and Dumesic, J. A., *in* "Studies in Surface Science and Catalysis" (B. Imelik, C. Naccache, G. Coudurier, H. Praliaud, P. Meriaudeau, P. Gallezot, G. A. Martin, and J. C. Vedrine, Eds.), Vol. 11, p. 43. Elsevier, Amsterdam, 1982.
12. Emmett, P. H., *in* "The Physical Basis for Heterogeneous Catalysis" (E. Dranglis and R. I. Jeffe, Eds.), p. 3. Plenum, New York, 1975.
13. Broden, G., and Bonzel, H. P., *Surf. Sci.* **84,** 106 (1979).
14. Ertl, G., Lee, S. B., and Weiss, M., *Surf. Sci.* **114,** 527 (1982).
15. Ertl, G., Weiss, M., and Lee, S. B., *Chem. Phys. Lett.* **60,** 391 (1979).
16. Doyen, G., and Ertl, G., *Surf. Sci.* **69,** 157 (1977).
17. Aika, K. I., Yamaguchi, J., and Ozaki, A., *Chem. Lett. (Japan)* **2,** 161 (1973).
18. Nobile, Jr., A., and Davis, Jr., M. W., *J. Catal.* **116,** 32 (1989).
19. Tau, L. M., and Bennett, C. O., *J. Catal.* **89,** 285 (1984).
20. Kolthoff, I. M., and Sandell, E. B., "Textbook of Quantitative Inorganic Analysis," Macmillan, New York, 1936.
21. Mears, D. E., *Ind. Eng. Chem. Process Des. Dev.* **10,** 541 (1971).
22. Nobile, A., Ph. D. dissertation, University of South Carolina, 1986.
23. Brunauer, S., and Emmett, P. H., *J. Amer. Chem. Soc.* **57,** 1754 (1935).
24. Emmett, P. H., and Brunauer, S., *J. Amer. Chem. Soc.* **59,** 1553 (1937).
25. Cameron, S. D., and Dwyer, D. J., *Langmiur* **4,** 282 (1988).
26. Cullity, B. D., "Elements of X-Ray Diffraction," Addison–Wesley, Menlo Park, CA, 1956.
27. Warren, B. E., *J. Appl. Phys.* **12,** 375 (1941).
28. Anderson, J. R., "Structure of Metallic Catalysts," Academic Press, New York, 1975.
29. Temkin, M. I., *Adv. Catal.* **28,** 173 (1979).
30. Nielsen, A., Kjaer, J., and Hansen, B., *J. Catal.* **3,** 68 (1964).
31. Bokhoven, C., van Heerded, C., Westrik, R., and Zwietering, P., *in* "Catalysis" (P. H. Emmett, Ed.), Vol. 3. Reinhold, New York, 1955.
32. Brill, R., *J. Chem. Phys.* **19,** 1047 (1951).
33. Holzmann, P. R., Shiflett, W. K., and Dumesic, J. A., *J. Catal.* **62,** 167 (1980).
34. Rambeau, G., Amariglio, H., *J. Catal.* **72,** 1 (1981).
35. A. A. Ray, Ed., "SAS Users Guide: Statistics." SAS Institute, Cary, NC, 1982.
36. Wynblatt, P., and Gjostein, N. A., *in* "Progress in Solid State Chemistry" (J. O. McCaldin and G. Somerjai, Eds.), Vol. 9. Pergamon, New York, 1975.
37. Wanke, S. E., and Flynn, P. C., *Catal. Rev. Sci. Eng.* **10,** 93 (1975).
38. Wanke, S. E., and Flynn, P. C., *J. Catal.* **34,** 390 (1974).
39. Wanke, S. E., and Flynn, P. C., *J. Catal.* **34,** 400 (1974).

40. Ruckenstein, E., and Pulvermacher, B., *AIChE J.* **19**(2), 356 (1973).
41. Ruckenstein, E., and Pulvermacher, B., *J. Catal.* **29,** 224 (1973).
42. Lemaitre, J. L., Menon, P. G., and Delannay, F., *in* "Characterization of Heterogeneous Catalysts" (F. Delannay, Ed.), p. 299. Dekker, New York, 1984.
43. Kingery, W. D., *J. Amer. Ceram. Soc.* **36**(11), 362 (1953).
44. Kingery, W. D., *J. Amer. Ceram. Soc.* **37**(2), 42 (1954).
45. Humenik, Jr., M., and Kingery, W. D., *J. Amer. Ceram. Soc.* **37**(1), 18 (1954).
46. Pillar, R. M., and Nutting, J., *Philos. Mag.* **16,** 181 (1967).
47. Dean, J. A., Ed., "Lange's Handbook of Chemistry, 12th Edition," McGraw–Hill, New York, 1979.
48. Box, G. E. P., Hunter, W. G., and Hunter, J. S., "Statistics for Experimenters," Wiley, New York, 1978.
49. Tauster, S. J., Fung, S. C., and Garten, R. L., *J. Amer. Chem. Soc.* **100,** 170 (1978).
50. Tauster, S. J., and Fung, S. C., *J. Catal.* **55,** 29 (1978).
51. Horsley, J. A., *J. Amer. Chem. Soc.* **101,** 2870 (1979).
52. Sexton, B. A., Hughes, A. E., and Foger, K., *J. Catal.* **77,** 85 (1982).
53. Chien, S. H., Shelimov, B. N., Resasco, D. E., Lee, E. H., and Haller, G. L., *J. Catal.* **77,** 301 (1982).
54. Kao, C. C., Tsai, S. C., Bahl, M. K., Chung, Y. W., and Lo, W. J., *Surf. Sci.* **95,** 1 (1980).
55. Baker, R. T. K., Prestridge, E. B., and Garten, R. L., *J. Catal.* **56,** 390 (1979).
56. Baker, R. T. K., Prestridge, E. B., and Garten, R. L., *J. Catal.* **59,** 293 (1979).
57. Simoens, A. J., Baker, R. T. K., Dwyer, D. J., Lund, C. R. F., and Madon, R. J., *J. Catal.* **86,** 359 (1984).
58. Sadeghi, H. R., and Henrich, V. E., *J. Catal.* **87,** 279 (1984).
59. Spencer, M. S., *J. Catal.* **93,** 216 (1985).
60. Resasco, D. E., and Haller, G. L., *J. Catal.* **82,** 279 (1983).
61. Jiang, X. Z., Hayden, T. F., and Dumesic, J. A., *J. Catal.* **83,** 168 (1983).
62. Raupp, G. B., and Dumesic, J. A., *J. Catal.* **97,** 85 (1986).
63. Littrell, D. M., and Tatarchuk, B. J., *J. Vac. Sci. Technol.* **4**(3), 1608 (1986).
64. Herrmann, J., and Pichat, P., *J. Catal.* **78,** 425 (1982).
65. Emmett, P. H., and Brunauer, S., *J. Amer. Chem. Soc.* **59,** 310 (1937).
66. Paál, Z., Ertl, G., and Lee, S. B., *Appl. Surf. Sci.* **8,** 231 (1981).
67. Silverman, D. C., and Boudart, M., *J. Catal.* **77,** 208 (1982).
68. Chen, H. C., and Anderson, R. B., *J. Catal.* **28,** 161 (1973).
69. Brunauer, S., Love, K. S., Keenan, R. G., *J. Amer. Chem. Soc.* **64,** 751 (1942).
70. Kock, A. J. H. M., and Geus, J. W., *Prog. Surf. Sci.* **20**(3), 165 (1985).
71. Heskett, D., *Surf. Sci.* **199,** 67 (1988).
72. Chai, G. Y., and Falconer, J. L., *J. Catal.* **93,** 152 (1985).